J. Mol. Biol. (1985) **184**, 645–656

Constraints on Flagellar Rotation

Shahid Khan, Markus Meister and Howard C. Berg

Division of Biology 216–76, California Institute of Technology
Pasadena, CA 91125, U.S.A.

(Received 15 October 1984, and in revised form 26 February 1985)

The motion of tethered cells of *Streptococcus* was analyzed at low values of protonmotive force (Δp). Cells repeatedly energized and de-energized stopped at discrete angular positions, indicating a rotational symmetry of barriers to rotation of order 5 or 6. At values of Δp smaller than -30 mV, constraints imposed by these barriers were evident when cells were starved and gradually energized, but not when they were energized first and then gradually de-energized. At values of Δp larger than about -30 mV, the cells behaved as if there were no barriers. Cells spinning in this regime also executed rotational Brownian movement. At energy levels above threshold, the motor determines torque; it does not fix the position of the rotor relative to the stator.

1. Introduction

A bacterial flagellum is driven at its base by a reversible rotary motor (Berg & Anderson, 1973; Silverman & Simon, 1974; Berg, 1975) comprising a pair of rings mounted on a rod linked to the flagellar filament by the proximal hook (Dimmitt & Simon, 1971; DePamphilis & Adler, 1971). Power is supplied by a protonmotive force (Δp), not by ATP (Larsen *et al.*, 1974): metabolizing cells can be stopped by the simultaneous addition of agents that collapse a transmembrane potential difference ($\Delta\psi$) and a transmembrane pH difference (ΔpH), but not by such agents when added separately (Skulachev, 1975; Belyakova *et al.*, 1976; Manson *et al.*, 1977); starved cells can be started up by artificial application of either $\Delta\psi$ or ΔpH (Manson *et al.*, 1977; Matsuura *et al.*, 1977; Glagolev & Skulachev, 1978).

When cells are tethered to glass by a single flagellum, they spin alternately clockwise and counterclockwise (Silverman & Simon, 1974) at a rate proportional to the torque generated by the flagellar motor (Berg, 1974). This technique has been used with the motile *Streptococcus* strain V4051 (van der Drift *et al.*, 1975) to establish a number of dynamic and energetic properties of the motor (Manson *et al.*, 1980; Berg *et al.*, 1982; Khan & Berg, 1983). Among these is the observation that when cells are completely de-energized (when $\Delta p = 0$), their motors remain rigidly engaged most of the time, but when they are energized to a small extent ($|\Delta p| < kT/e = 25$ mV, where k is Boltzmann's constant, T is the absolute temperature, and e is the proton charge) they spin steadily. Evidently, the action of several protons is required to carry the motor past barriers to rotation (Manson *et al.*, 1980; Berg *et al.*, 1982).

In the work reported here, we have taken a closer look at these barriers by examining the rotational behavior of tethered cells at low protonmotive force (0 to 3 kT/e). We have found that the barriers are spatially periodic. Their amplitudes depend on cell history. The effects of barriers are not apparent at energy levels well above threshold, where variations in period appear to arise from free rotational Brownian movement. The flagellar motor determines torque, not angular position.

2. Materials and Methods

(a) *Tethering*

Cells of *Streptococcus* strain V4051 or SM197 (Berg *et al.*, 1982) were grown, washed 4 times in standard buffer (0·1 M-sodium phosphate (pH 7·5), 0·2 M-KCl, 10^{-4} M-EDTA), tethered to a silanized glass coverslip, and placed in a miniature flow-cell (Berg & Block, 1984), as described previously (Manson *et al.*, 1980). Growth was at 35°C, but all subsequent manipulations were at room temperature (22°C). Cells of strain SM197 spin exclusively counterclockwise (when tethered to a slide and viewed from above) when protons are driven inward; therefore, measurements of rotation rates with this strain are not complicated by reversals (see Khan & Berg, 1983).

(b) *Energization*

In most experiments, tethered cells were energized with a potassium diffusion potential. Once starvation was complete (after about 1 h, as evidenced by total cessation of rotation), the cells were pretreated with valinomycin (2 μg/ml in standard buffer for 1 min). Beginning about 5 min later, they were shifted to media containing lower

0022-2836/85/160645-12 $03.00/0

concentrations of potassium ion (standard buffer with part of the KCl replaced by NaCl). Complete exchanges of media were effected by 10 s flows through a needle valve connected to a vacuum line or by use of a peristaltic pump (Gilson Minipuls 2). We followed the standard sign convention and assigned positive values to $\Delta\psi$ or ΔpH when the inside of the cell was at a positive potential or acid relative to the outside of the cell. Accordingly, the cells in this study were energized at negative values of Δp. In experiments involving increased viscous loads, Ficoll 400 (Pharmacia) was added to the media from concentrated stock solutions (Berg & Turner, 1979) purged of metabolizable contaminants by passage through Sephadex G-50.

In ramp experiments, the concentration of KCl was lowered continuously by flow of potassium-free medium into a mixing chamber (net volume 0·7 ml) containing a small magnetically driven stirring bar. The chamber was filled initially with standard buffer. The output of the mixer was connected to 3 ports: 1 leading to the input of the flow-cell, 1 leading to a peristaltic pump (Gilson Minipuls 2), and 1 leading to a small mercury manometer. Fluid was drawn out of the flow-cell with a second peristaltic pump (Holter RA034) at the rate of about 0·05 ml/min, the first pump was run at the rate of about 1·4 ml/min, and the level of the reservoir supplying the potassium-free medium was adjusted so that the pressure sensed by the manometer was slightly less than atmospheric. This was done to ensure that the coverslip remained properly seated on the flow-cell. Since with this setup the concentration of potassium ion falls exponentially with time, and the Nernst potential for potassium is logarithmic in concentration, the cells are exposed to a potassium diffusion potential the magnitude of which increases linearly with time (for the mixing chamber volume and flow-rates given, at the rate of about 0·8 mV/s). The system was calibrated (and this expectation was confirmed) by replacing the flow-cell with a potassium electrode of similar volume (constructed from Orion sensing electrode 93–19 and reference electrode 90–01, with the latter downstream from the former). Connections were made with the same lengths of polyethylene tubing (0·58 mm i.d.), so that the time-course of the potential change was determined accurately.

In experiments designed to find periodicities in stopping angles, cells were energized either with a potassium diffusion potential or with glucose. In the former case, the media were supplemented with sodium benzoate (0·025 M) and methylamine (0·05 M) to clamp ΔpH (Repaske & Adler, 1981; Kihara & Macnab, 1981); after treatment with valinomycin (as above), the cells were started by a shift to 0·05 M-KCl, 0·15 M-NaCl and stopped by a shift back to 0·2 M-KCl. The addition of benzoate and methylamine ensured that the cells stopped within seconds of the latter shift. Cells energized with glucose (10^{-5} M) were stopped by a shift to standard buffer containing an uncoupler, 2,4-dinitrophenol (0·01 M). They also stopped within a few seconds of this buffer change. In either case, the cells could be started and stopped 30 to 40 times before a significant fraction came off the glass.

In pH-jump experiments, cells prepared in standard buffer at pH 8·5 were tethered to a quartz coverslip and exposed to a buffer containing 0·1 mM-sodium phosphate (pH 8·5), 0·1 M-NaCl, 0·2 M-KCl, 10^{-4} M-EDTA and 1 mM-2-hydroxyphenyl-1-(2-nitro)phenylethyl phosphate, a photolabile phosphate diester monoanion that liberates protons on exposure to near-ultraviolet light at 300 to 350 nm (McCray & Trentham, 1985). A pH jump of −0·73 unit was effected by a single flash of a xenon lamp (Chadwick-Helmuth Strobex model 238 supply and 278 lamp in an elliptical reflector behind a Schott WG 295 ultraviolet blocking filter, rated at 200 Ws in 0·1 ms) focused on the coverslip obliquely from above, as judged from absorbance changes of the pH indicator phenol red (0·2 mM) monitored with a photodiode detector (Block *et al.*, 1983). The pH-jump was complete in a time comparable to the duration of the flash (< 1 ms), as judged from measurements with the photomultiplier detector of the pinhole apparatus (Berg, 1976).

(c) *Data acquisition and analysis*

Most experiments were recorded on videotape by inverse phase contrast microscopy with a Nikon microscope (S-Ke with BM 40× objective), a Sanyo vidicon camera (VC1620×; 2 : 1 interlace) and a Panasonic VHS recorder (NV8950). In some experiments, calibration of the radius of gyration of the image (half the diameter of the circle swept out by the rotating cell) was made by comparison with a recording of an objective micrometer. Rotation periods were measured by a system linked to an Apple computer that timed intervals between transits of images over a video cursor. This system was calibrated by focusing the video camera on a white paper mockup of a cell that was spun with a stepping motor drive (Block *et al.*, 1983). Since the video scans occurred 60 times a second, there was an uncertainty of half the scan interval (8·5 ms) in every measurement of a rotation period. This expectation was confirmed in experiments with the mockup. The values of the standard deviation in the period observed for tethered cells were corrected for this instrumental uncertainty (by subtracting the instrumental variance from the total variance). Recordings of some cells that spun very slowly were played back at quarter speed and analyzed by eye. Crossings of a cursor were clocked by push button and strip chart event marker with a system developed for measurements of chemotactic responses (Block *et al.*, 1982, 1983). Once again, correction was made for the instrumental uncertainty, as determined from analysis of recordings of the spinning mockup.

In the experiments designed to find periodicities in stopping angles, a photograph of the field was taken every time the cells were stopped. We used an inverse phase contrast microscope (Nikon Optiphot with Plan BM 40× objective) and a Polaroid camera (Nikon PFX with CF PL 5× projection lens). Exposures of approx. 17 s were taken on positive/negative film (Polaroid 665). The negatives were viewed under a modified dissecting microscope. The difference in the orientation of the long axis of a given cell and a reference line connecting 2 widely spaced fixed objects in the field was determined with a universal bevel protractor. For most cells, the error in this measurement was between 1° and 2°. A cosine transform technique was used to analyze the stopping angles for periodicities. For a given cell, we computed the set of differences between successive stopping angles. Assuming that all cells operate with the same kind of motor, we pooled their difference angles and computed:

$$C(M) = \frac{1}{n} \sum_{j=1}^{j=n} \cos(M\phi_j), \qquad (1)$$

where ϕ_j, $j = 1, 2, \ldots, n$ are the difference angles. If the values of ϕ_j are distributed randomly, one expects $|C(M)|$ to be small and comparable for all values of M. If.

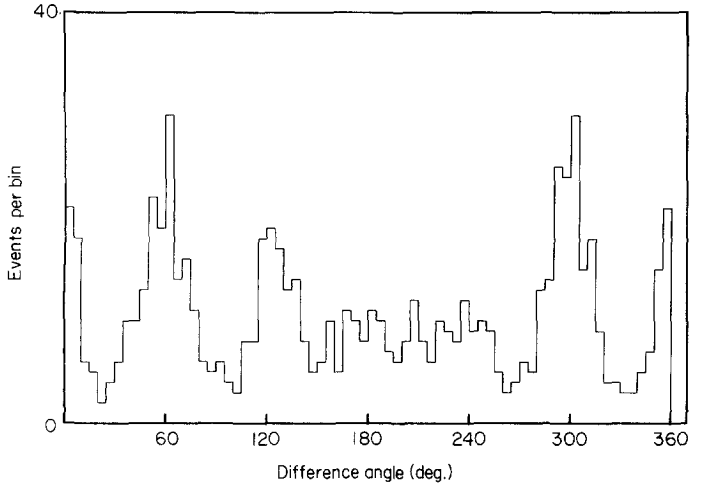

Figure 1. Histogram of differences between successive stopping angles of 21 cells of strain V4051 energized with glucose and stopped with 2,4-dinitrophenol. The angles (759 in number) were sorted in bins of width 5°.

however, the values of ϕ_j are distributed with a rotational periodicity of order L, then $C(M)$ will be large and positive if M is an integer multiple of L. The properties of $C(M)$ expected for these experimental conditions are derived in the Appendix.

Changes in rotation rate in the pH-jump experiments were followed with the pinhole apparatus described previously (Berg, 1976). Strip-chart recordings (125 mm/s) were made of the intensity of the image of a tethered cell as it crossed the pinhole. The flash generating the pH-jump (see above) was triggered by a comparator set to fire when this intensity was about 30% of maximum. Enough light was scattered into the microscope to mark this event on the analog record. The rotation rate of the cell was estimated from the interval between successive crossings. The lag between the flash and the subsequent change in rate was estimated by comparing tracings of earlier and later waveforms with that obtained at the time of the flash.

3. Results

(a) *Rotational barriers show a symmetry of order 5 or 6*

A histogram of the differences between successive stopping angles measured in an experiment in which cells of strain V4051 were energized with glucose is shown in Figure 1. The corresponding cosine transform, $C(M)$, is shown in Figure 2. In the latter plot, there are sizeable peaks at $M = 6$ and $M = 12$, indicating a rotational symmetry of order 6. From the ratio of the two peaks at $M = 6$ and $M = 12$, one finds (see Appendix) that the periodic stopping angles are defined to within a width of about $\sigma_\phi = 10°$. The large positive value of $C(1)$ and the large negative value of $C(3)$ reflect the bias toward small angles evident in the histogram of Figure 1. This bias is due to the fact that some cells stopped while aligned by the flow of the medium containing 2,4-dinitrophenol, and thus were found at similar angles, while others continued to spin after the flow was turned off, and thus chose their stopping angles at random.

Some cells continued to creep (at $< 0{\cdot}1$ Hz) during the exposure of the film. They sped up and slowed down in a periodic manner, producing images that were brighter in regions in which they moved more slowly. Some of these daisy-like images can be seen in Figure 3. Images of this kind had at most five or six petals, usually unevenly spaced. When energized, these same cells gave images without azimuthal structure.

In another experiment, with cells of strain V4051 energized by a potassium diffusion potential, the cosine transform showed significant peaks of approximately the same height both at $M = 5$ and $M = 6$. A third experiment using cells of strain SM197 energized with glucose gave the same result.

(b) *Rotational barriers depend on cell history*

We studied the relationship between rotation rate and protonmotive force near $\Delta p = 0$ in some detail. Cells were energized in a ramp experiment in which the potassium diffusion potential was increased linearly from 0 to 50 mV over a period of about one minute. The data for one cell are shown in Figure 4 and for an ensemble of eight cells in Figure 5. Most cells began to rotate at potentials of about -10 mV. Their speeds increased non-linearly with Δp. From about -30 mV onwards, the speeds extrapolated linearly backwards to 0 mV (-2 ± 6 mV). This implies that effects of barriers felt below -30 mV are no longer evident at larger potentials.

Alternatively, cells were energized by discontinuous shifts to media containing potassium at different concentrations. The magnitude of the protonmotive force could be increased or decreased. In the former case, the dependence of rotation rate on protonmotive force (Fig. 6, asterisks) was the

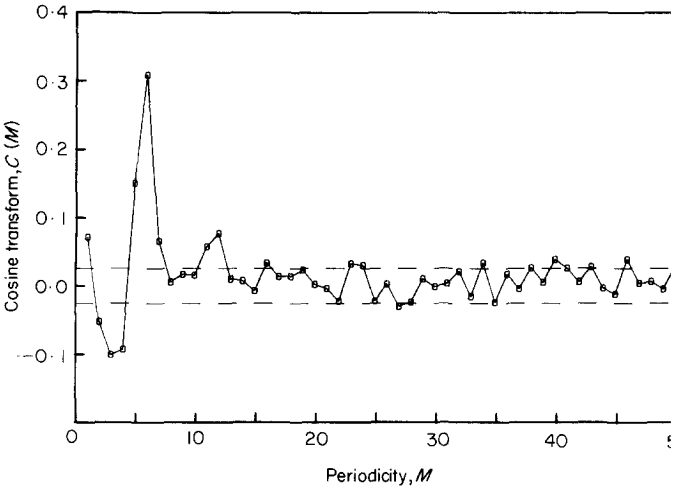

Figure 2. Cosine transform of the difference angles shown in Fig. 1. The broken lines indicate the noise level expected with a random set of stopping angles (see Appendix).

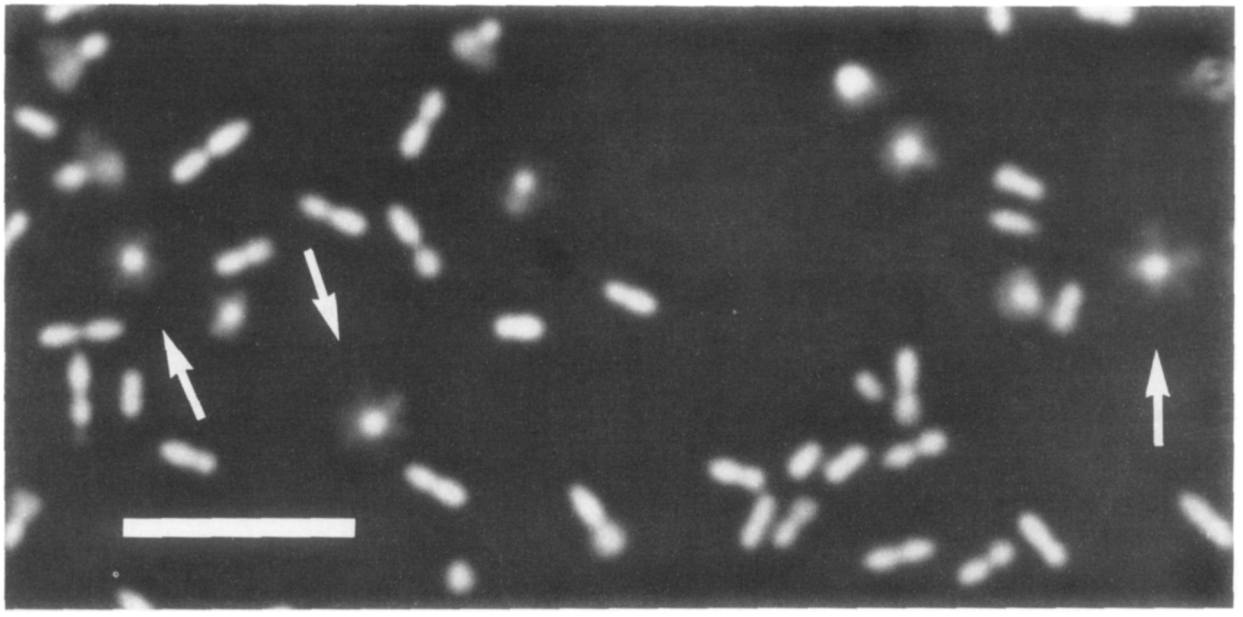

Figure 3. Part of one of the photomicrographs from the start–stop experiment of Figs 1 and 2 (exposure time 17 s). Note the daisy-like patterns produced by creeping cells (arrows). The direction of flow was from left to right. The bar represents 20 μm.

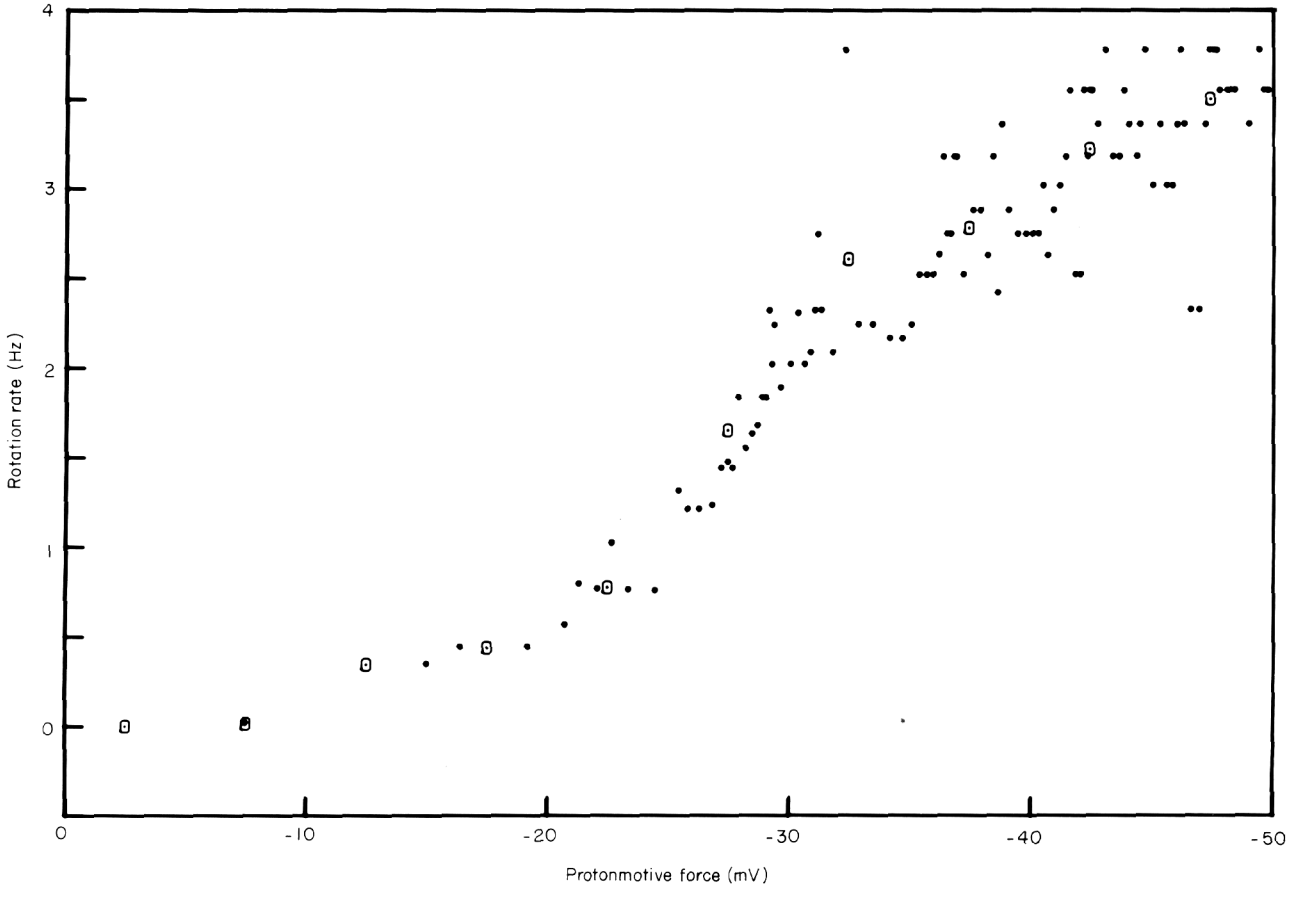

Figure 4. Rotation rate of a cell of strain SM197 exposed to an increasing ramp in diffusion potential. The dots are rotation rates computed from measurements of successive rotation periods, placed at values of protonmotive force inferred from calibration of the external potassium concentration. The circles are mean values for the rates in bins of width 5 mV.

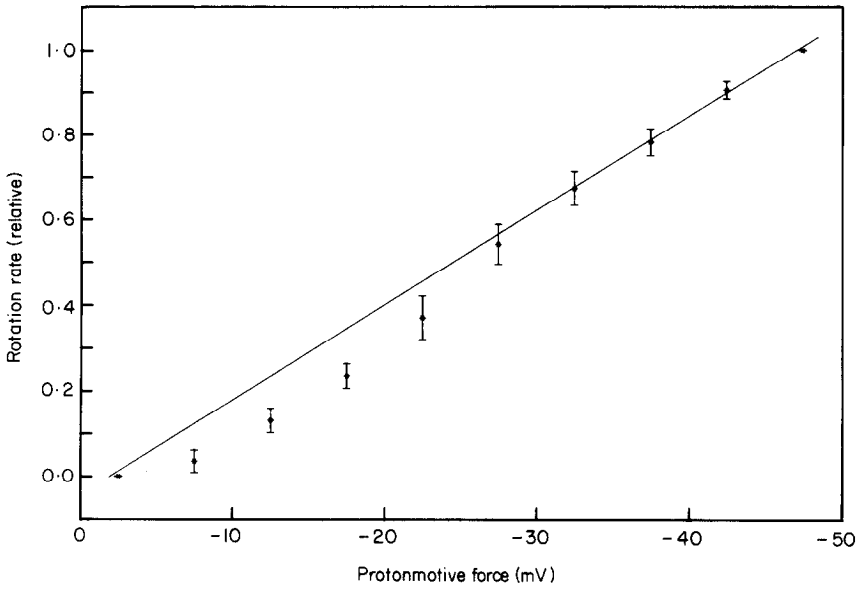

Figure 5. Relative rotation rate as a function of diffusion potential for 8 cells obtained from data of the kind shown in Fig. 4. The mean value of the rate for each cell in each bin was scaled to the maximum mean value for that cell. These data were combined, with each cell weighted equally. The asterisks are the ensemble means, and the bars are the standard errors. The line is a weighted least-squares fit to the data over the range −30 to −50 mV (assigning a standard error to the mean in the last bin equal to the mean of the standard errors for the 3 preceding bins; slope and standard deviation −0·022 (±0·003), ordinate intercept and standard deviation −0·042 (±0·127), correlation coefficient 0·998). The mean rotation rate of the 8 cells at −47·5 mV and its standard deviation were 3·07 (±1·00) Hz.

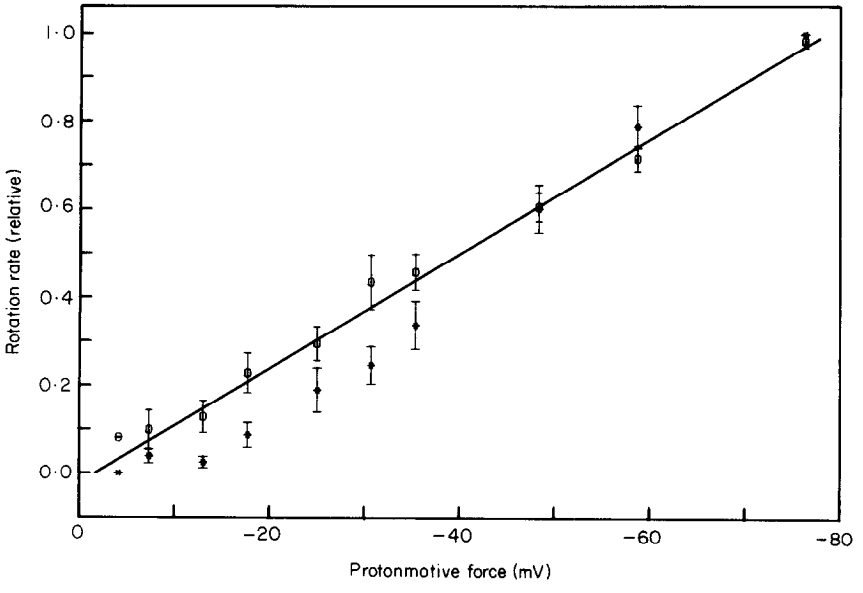

Figure 6. Differences in rotation rates of cells of strain SM197 subjected to large and then progressively smaller potassium diffusion potentials (circles) or to small and then progressively larger potassium diffusion potentials (asterisks). A set of 10 cells was studied, each cell of which spun at the end of the experiment (when energized at −76 mV) at about the same rate that it did when energized at this potential earlier in the experiment. The first 5 cells were exposed to a protonmotive force of −76 mV and then shifted step by step to 0 mV and back again, while the second 5 were shifted step by step from 0 mV to −76 mV and then back again. The data for the downward steps (circles) were analyzed separately from the data for the upward steps (asterisks). The rotation rates for each cell were scaled to the corresponding rate at −76 mV. The scaled rates were weighted equally: the symbols are the means, the bars are the standard errors. The line is a weighted least-squares fit to the data for the downward steps (excluding the data points below −10 mV and assigning a standard error to the point at −76 mV equal to the mean of the standard errors of the 3 neighboring points; slope and standard deviation −0·013 (±0·001); ordinate intercept and standard deviation −0·022 (±0·029); correlation coefficient 0·997). The mean rotation rate of the 10 cells at −76 mV and its standard deviation were 3·01 (±1·44) Hz.

same as that observed in the ramp experiments (Fig. 5). However, in the latter case, when the magnitude of the protonmotive force was decreased, the rotation rate was a linear function of protonmotive force down to an apparent threshold of about $-2(\pm 2)$ mV (Fig. 6, circles). Constraints due to barriers to rotation were no longer evident.

Other evidence for the kind of changes apparent in Figure 6 was obtained in experiments on temperature dependence described earlier (Khan & Berg, 1983). Starved cells cooled from room temperature to 4°C and energized within about one minute ($\Delta p \simeq -80$ mV) generated torques that were close to those observed at room temperature. However, cells that were cooled to 4°C and held at that temperature for several minutes before being energized generated torques that were substantially smaller. When cooled only a few degrees further, the cells failed to spin at all. The barriers to rotation changed with time.

In an effort to define these barriers further, we turned to an analysis of the time dependence of changes in rate following abrupt pH-jumps (generated photolytically). It took much longer for cells to start up when stopped than to change speeds when spinning rapidly. For example, one cell took about 0·7 second to start up when exposed to a jump of $-0{\cdot}73$ unit (-43 mV), after which time it accelerated rapidly to 1·3 Hz. However, when energized first with a potassium diffusion potential and spinning at 3·6 Hz, a similar jump caused it to increase its speed within about 0·03 second by 1·8 Hz. Data for a second cell are shown in Figure 7. When this cell spun 0·1 Hz or faster, changes in its speed occurred much more rapidly. The cell did not accelerate at widely different rates, but rather delayed the onset of the change by different times and then accelerated abruptly. Note that the long lags occurred at initial values of $|\Delta p| < 10$ mV.

Changes in speed could be generated also by abrupt shifts in the potassium diffusion potential. Cells energized at a diffusion potential of 76 mV were exposed to an iontophoretic pipette (Segall *et al.*, 1982) containing 1 M-KCl. Cells spinning at rates of 1 Hz or higher slowed down or sped up when the pipette was turned on or off, with lags of less than 0·1 second (as judged by eye on slow-speed playback of a video recording). Cells spinning at lower speeds were not studied.

(c) *At energy levels above threshold, cells are free to execute rotational Brownian movement*

We were led to this conclusion by a three-part stochastic analysis, in which we studied the standard deviation in rotation period as a function of mean period at different membrane potentials, viscous loads, and number of revolutions per interval.

(i) *Standard deviation in rotation period as a function of mean period at different membrane potentials*

The raw data were a series of measurements of successive rotation periods of mean duration τ, standard deviation σ_τ, as shown in Figure 8. A cell free to execute rotational Brownian movement will advance or retreat, during a time interval τ, a root-mean-square angle $\theta = (2D_r\tau)^{1/2}$, where D_r is the rotational diffusion coefficient of the cell (Berg, 1983). As a result, the image of the cell will reach the cursor earlier or later than otherwise would be the case, shortening or lengthening the observed period. The error in cycles is $\theta/2\pi$, and the mean

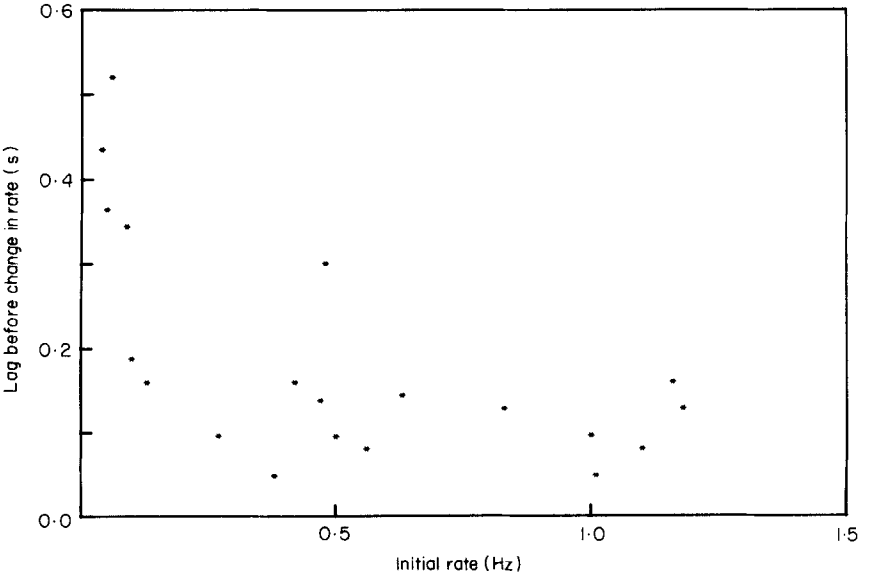

Figure 7. The lag time before changes in rate of a tethered cell of strain SM197 energized to varying degrees with a potassium diffusion potential and then subjected to a sudden negative pH-jump of 0·73 units ($\Delta p = -43$ mV). In all cases, this jump increased the rotation rate of the cell by about 1 Hz. The protonmotive force at 0·2 Hz (below which the lag was substantial) was, thus, about -10 mV.

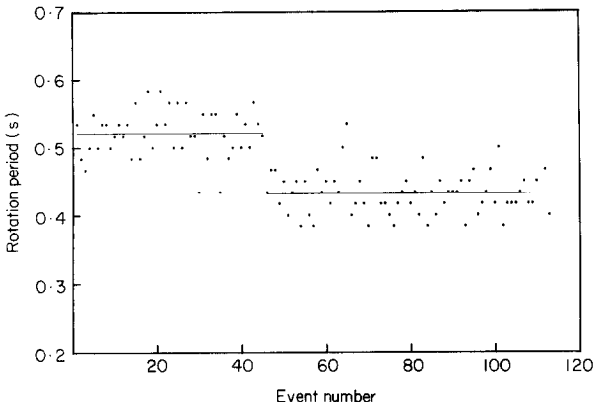

Figure 8. The kind of data obtained from transits of an image of a tethered cell over a video cursor. Successive rotation periods are shown (dots). The points appear on lines 17 ms apart, the interval between successive video scans. The mean for the first 45 events (spanning 23·4 s) and its standard deviation were 0·521 (±0·034) s: the mean is indicated by the upper horizontal line. The mean for the next 67 events (spanning 28·9 s) and its standard deviation were 0·431 (±0·032) s: this mean is indicated by the lower horizontal line. The number of events included in a given set of measurements ranged from about 10 to more than 100, depending upon the time available and whether or not the mean remained substantially constant.

period per cycle is τ, so the error (standard deviation) in τ, $(\theta/2\pi)\tau$, is:

$$\sigma_\tau = (D_r/2\pi^2)^{1/2}\tau^{3/2}. \quad (2)$$

We studied this relationship by shifting cells to media at different potassium concentrations, measuring the rotation period for each cell and its standard deviation at different values of proton-motive force. A two-parameter fit was made for each of 15 cells to the relation $\sigma_\tau = a\tau^b$. The mean value of b and its standard error were $1{\cdot}39 \pm 0{\cdot}10$, consistent with the value 3/2. This encouraged us to test equation (2) more directly by making a single parameter fit to the relation $\sigma_\tau = a_1\tau^{3/2}$. The weighted mean value for a_1 and its standard error were $(0{\cdot}119 \pm 0{\cdot}009)$ $s^{1/2}$. The rotational diffusion coefficient deduced from this value, equation (2), is 0·28 radians^2/second. This is the rotational diffusion coefficient of a sphere of diameter 1·7 μm, an object roughly the size of a tethered cell. The parameter a_1 should vary with the radius of gyration of the cell, r: it should be substantially smaller for large cells than for small cells. This dependence is shown in Figure 9, which indicates that a_1 is roughly proportional to $r^{-0{\cdot}80}$.

The speed of cells running at constant torque is inversely proportional to the rotary viscous drag coefficient, kT/D_r (Berg, 1983). Assuming that the torque is constant, this has been shown to be a reasonable assumption for metabolizing cells (Manson *et al.*, 1980) and for cells energized with a potassium diffusion potential (at −76 mV, unpublished data). It follows that the functional dependence of rotational diffusion coefficient on cell size can be determined from measurements of the dependence of speed on cell size. For this purpose, we returned to the data used to prepare Table 1 of Manson *et al.* (1980) and examined log–log plots of rotation rate *versus* radius of gyration for 64 cells energized with a potassium diffusion potential of −76 mV and 88 cells energized with a potassium diffusion potential of −59 mV. Both plots were

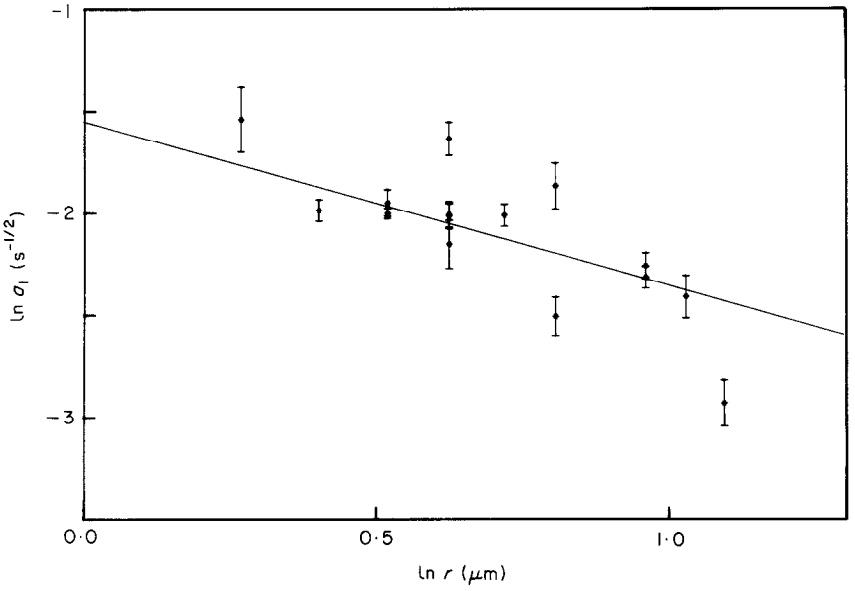

Figure 9. Dependence of the parameter $a_1 = (D_r/2\pi^2)^{1/2}$, eqn (2), on the radius of gyration, r. A total of 124 measurements were made on 15 cells of strain SM197 energized at potassium diffusion potentials ranging from −35 to −135 mV. Fits of the relation $\sigma_\tau = a_1\tau^{3/2}$ were made to the data for each cell. The error bars are estimates of the standard deviations in a_1. A log–log plot is shown of a_1 as a function of the radius of gyration. The line is a weighted least-squares fit, with slope −0·80. The large scatter in this plot probably is due to variables other than r that affect the rotational diffusion coefficient of a cell, e.g. cell diameter or tethering geometry.

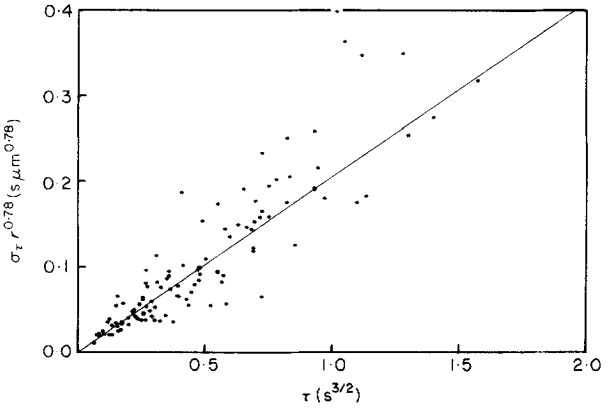

Figure 10. Dependence of $\sigma_\tau r^{0.78}$ on $\tau^{3/2}$, eqn (3). The data points are from the 15 cells of Fig. 9. Nine of these were off-scale and are not shown. The standard deviations belonging to different mean periods for a given cell (in s) were multiplied by the radius of gyration for that cell (in μm) raised to the 0·78th power and plotted as a function of the 1·5th power of the mean periods. The line is a least-squares fit to all 124 points, constrained at the origin, with slope and standard deviation 0·21 ($\pm$0·01).

readily fit by straight lines (correlation coefficients 0·99), with slopes and standard deviations $-1{\cdot}48$ ($\pm$0·11) and $-1{\cdot}67$ ($\pm$0·13), respectively, yielding a weighted mean and standard deviation of $-1{\cdot}56$ ($\pm$0·08). Thus, to a fairly good approximation, the rotational diffusion coefficient of *Streptococcus* is proportional to the $-1{\cdot}56$th power of its radius of gyration. Thus, $D_r^{1/2}$ should be proportional to $r^{-0.78}$, in agreement with the size dependence found in Figure 9. Assuming the dependence $r^{-0.78}$, we pooled the data from all 15 cells and obtained the fit shown in Figure 10. We conclude from this study that the expectations of equation (2) are met.

(ii) *Standard deviation in rotation period as a function of mean period at different viscous loads*

The work that the flagellar motor does in driving the cell body through one revolution is the angular displacement, 2π, times the torque, $(kT/D_r)(2\pi/\tau)$. This work equals the efficiency of the motor, ε, times the energy available from the protons as they move down their electrochemical gradient, $Ne\Delta p$, where N is the number of protons that pass through the motor in one revolution. Thus, $D_r = 4\pi^2 kT/\varepsilon Ne\Delta p\tau$. Substitution in equation (2) gives:

$$\sigma_\tau = (2kT/\varepsilon Ne\Delta p)^{1/2}\tau. \qquad (3)$$

We studied this relationship by energizing cells at a fixed protonmotive force (-76 mV) and shifting them to media of different viscosities. A two-parameter fit was made for each of 20 cells to the relation $\sigma_\tau = a\tau^b$. The mean value of b and its standard error were 0·93 ($\pm$0·07), consistent with the value 1. This encouraged us to make a single-parameter fit to the relation $\sigma_\tau = a_2\tau$. The weighted mean value of a_2 and its standard error were 0·055 ($\pm$0·003), indicating a value for εN in equation (3) of 222 ($\pm$12). The parameter a_2 should be independent of the size of the cell, which appeared to be the case (Fig. 11). A linear least-squares fit to a plot of σ_τ *versus* τ made with the data from all 20 cells (Fig. 12) gave $a_2 = 0{\cdot}058$. We conclude from

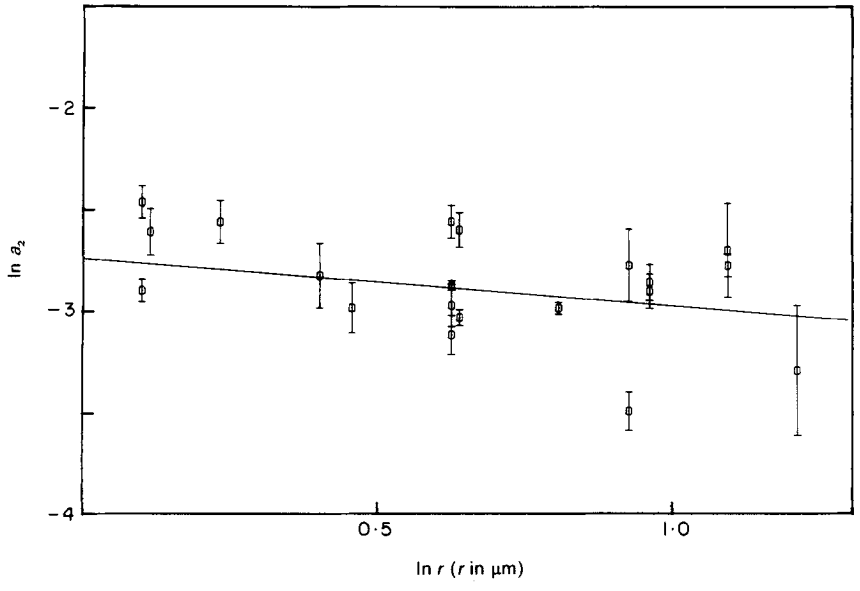

Figure 11. Dependence of the parameter $a_2 = (2kT/\varepsilon Ne\Delta p)^{1/2}$, eqn (3), on the radius of gyration. A total of 98 measurements were made on 20 cells of strain SM197 shifted to media containing different concentrations of Ficoll. Fits of the relation $\sigma_\tau = a_2\tau$ were made to the data for each cell. The error bars are estimates of the standard deviations in a_2. A log–log plot is shown of a_2 as a function of the radius of gyration. The line is a weighted least-squares fit, with slope $-0{\cdot}24$. The large scatter in this plot probably is due to differences from cell to cell of parameters that affect ε or Δp, e.g. membrane proton permeability.

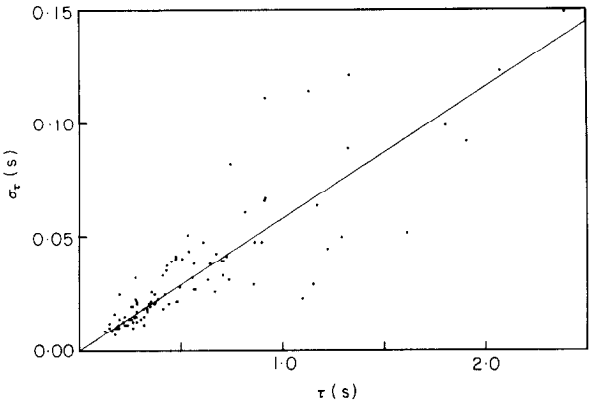

Figure 12. Dependence of σ_τ on τ, eqn (3). The data points are from the 20 cells of Fig. 11. The line is a least-squares fit constrained at the origin, with slope and standard deviation 0·058 (±0·002).

this study that the expectations of equation (3) are met also.

(iii) *Variance in rotation interval as a function of the number of revolutions per interval*

Additional information was extracted from the angular drift of a given cell over a large number of rotation periods. Returning to the arguments that led to equation (2), we note that a cell free to execute rotational Brownian movement will advance or retreat during a time interval $\alpha\tau$ a root-mean-square angle $(2D_r\alpha\tau)^{1/2}$. The standard deviation in the interval $\alpha\tau$ is this value times $\tau/2\pi$. The variance:

$$\sigma^2_{\alpha\tau} = (D_r\tau^3/2\pi^2)\alpha, \qquad (4)$$

is proportional to α. Plots of variance as a function of α are shown for two cells in Figure 13. Using the figures for the initial slopes and the mean periods given in the Figure legend, the rotational diffusion coefficients for the two cells are estimated to be 0·67 and 0·49 radians^2/second (upper and lower curves, respectively), corresponding to a sphere of diameter about 1·3 μm. Both plots in Figure 13 curve slightly upwards. This is due to long-term correlations (drift) in the data; both cells gradually increased and decreased their speed over spans of about one minute, intervals much longer than those used to measure τ in the studies relevant to equations (2) and (3). This was confirmed by adding extra drift to the data and noting the increase in curvature. The drift must be due to a process other than rotational Brownian movement.

From time to time, for no apparent reason, cells also rapidly shifted their rotation periods up or down by about 20 to 30%, a value substantially larger than the initial or final standard deviations. Sometimes this happened within one rotation period (Fig. 8 is a record of such an event) sometimes over an interval of several periods. When this occurred in the studies relevant to equations (2) and (3), the two intervals were analyzed separately

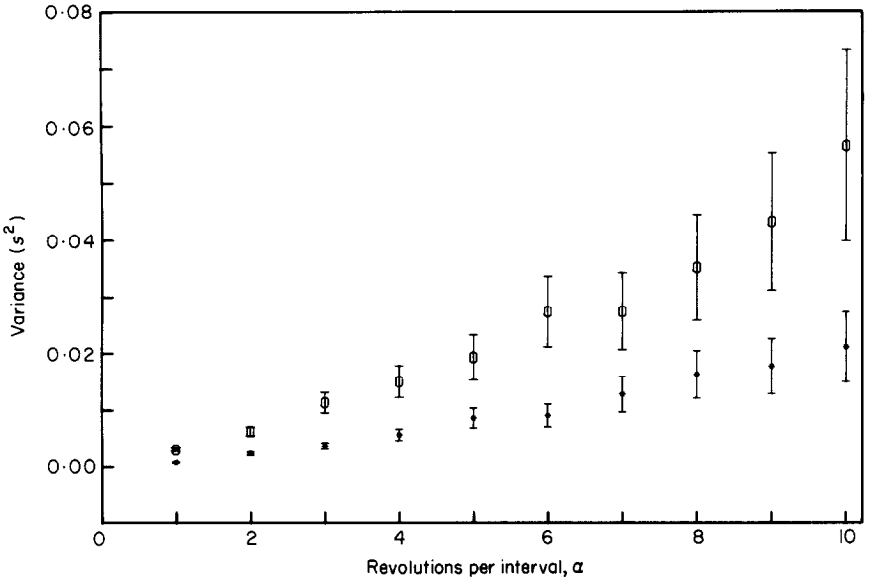

Figure 13. Variance in rotation interval as a function of the number of revolutions per interval for 2 medium-sized cells of strain V4051 energized by a potassium diffusion potential of −76 mV. The mean rotation periods for the first (circles) and second cell (asterisks) were 0·451 and 0·319 s, respectively; the data points were computed from measurements of 244 and 258 successive rotation periods, respectively. A least-squares straight-line fit was used to correct for the linear drift in period (the cells were slowing down) and the mean and variance were then computed for individual periods, sums of 2 successive periods, sums of 3 successive periods, etc. The initial slopes, judged from the data points at $\alpha = 1$, were $3{\cdot}11 \times 10^{-3}$ and $8{\cdot}06 \times 10^{-4}$ s^2, respectively. The error bars show 1 standard deviation of the variance expected if individual rotation periods were uncorrelated and distributed normally. They indicate that the curvature of the 2 plots is significant (see the text). The images of the 2 cells had about the same radius of gyration; the magnification was not determined.

(as shown in Fig. 8). The fractional change in period was found to be roughly constant for an ensemble of 24 cells with periods ranging from 0·2 to 1·0 second. These shifts were not correlated with changes in the orientation of the cells, which would be expected to change the viscous load. Polaroid time exposures of video images of several cells were made before and after such shifts, and the paired pictures were superimposable.

4. Discussion

Previous studies of the periodicity of flagellar motion were limited to an analysis of the variation of speed of spinning cells (tethered *Escherichia coli*). No periodicities were found; however, the search was hampered by elastic filtering due to the tether (Berg, 1976; Berg *et al.*, 1982). Elastic filtering was not a limitation in the measurements reported here, which were static (Figs 1 and 2) or nearly so (Fig. 3). We found periodicities of order 5 or 6.

A possible explanation of this mixed symmetry is indicated by structural studies of the flagellar hook in *Caulobacter crescentus* and *Salmonella typhimurium* (Wagenknecht *et al.*, 1981). Monomers of the hook protein assemble in a helical lattice, with about 5·5 subunits per turn. A dramatic feature of the three-dimensional reconstruction is the presence of deep, broad helical grooves in the surface of the hook. A cross-section perpendicular to the axis of the hook shows these grooves as alternating dense and empty regions along the periphery. Due to the non-integral number of subunits per turn, this cross-section has no defined azimuthal symmetry: the separation of successive dense regions on the periphery varies, with a mean of approximately 65°. If rotation of the motor shaft were constrained by interaction between such grooves and components of the cell wall, the stopping angles would reflect the angular distribution of these dense regions. One would then expect the cosine transform to show a broad peak extending over $M = 5$ and $M = 6$, as we have observed. These periodicities cannot be due to anisotropies in the flexural rigidity of the hook or of the filament, because the flagellum of a tethered cell does not rotate relative to the glass. Note that these static measurements characterize the symmetry of the barriers to rotation, not necessarily that of the torque-generating machinery *per se*.

The only clue in the present work that the torque-generating machinery of *Streptococcus* might also have a rotational symmetry of order 5 or 6 was the observation that the cells occasionally changed their speeds by about 20 to 30%, which they might do on losing or gaining one or more force-generating units. An analysis of this kind in *E. coli* has suggested a full complement of 16 such units (Block & Berg, 1984), a number also thought to characterize the rotational symmetry of the M ring (DePamphilis & Adler, 1971). In *Streptococcus*, preliminary work with negatively stained preparations of motors in Triton X-100 (unpublished data) has revealed two rings on a long rod, as in other gram-positive bacteria (Dimmit & Simon, 1971; DePamphilis & Adler, 1971), but nothing is known about the rotational symmetry.

The periodic nature of the motion of cells creeping very slowly (Fig. 3) implies that the rotor moves under the influence of a periodic potential due to interactions with the stator or other components of the cell wall. The non-linear behavior of speed as a function of Δp for cells that are shifted from small to larger values of Δp (Figs 4, 5 and 6 (asterisks)) is consistent with a mechanism in which a torque proportional to Δp is added to the periodic torque due to these barriers. As long as the torque generated by the motor is smaller than or comparable to the opposing torque of the barriers, the periodic potential merely slows the motion during one part of the cycle and speeds it up during the other. At very high Δp, one expects the periodic potential to have relatively little effect.

We had expected barriers to rotation to be fixed, but this was not the case. Indeed, cells energized at protonmotive forces larger than about −40 mV and then de-energized behaved as if there were no barriers to rotation: a plot of rotation rate as a function of protonmotive force was linear with an intercept not significantly different from 0 (Fig. 6 (circles)). The hysteresis evident in Figure 6, the time-dependent effects on rotation rate noted with cells artificially energized at low temperature, and the non-linear lag in response to jumps in pH (Fig. 7), all point to processes involving changes in structure. It might be, for example, that particulate material gets stuck between the cell wall and the grooves and ridges of the drive shaft, blocking rotation. Once this grit is dislodged mechanically, the motor can spin freely. However, when the motor is de-energized and rotation stops, this material accumulates again, and the barriers to rotation are restored.

Delays in initiation of motility also have been observed in the photosynthetic bacterium *Rhodopseudomonas sphaeroides* (Armitage & Evans, 1982). The lag between light-induced energization and onset of swimming of cells that had been incubated anaerobically in the dark varied from seconds to minutes, depending inversely on the magnitude of the change in membrane potential, as judged from carotenoid bandshifts. It was postulated that the protonmotive force alone is not enough for initiation of flagellar rotation. Our data suggest that the problem lies not in torque generation *per se*, but rather in overcoming barriers to rotation. The smallest delays observed in changing rotation rates of spinning cells (about 30 ms) were comparable to the time-resolution of the recording system, so we do not know whether these delays are significant. Clearly, more work needs to be done on these non-linear effects.

Beyond −30 to −40 mV, speed was proportional to Δp regardless of how the cells were energized (Figs 5 and 6). This implies that the mechanical

work performed by protons in driving the motor through one revolution is proportional to the protonmotive force; losses, if any, are not constant but also are proportional to protonmotive force.

Early work with tethered cells suggested that the coupling between the flagellum and the body of the cell was rigid (Berg, 1974). As noted later (Berg, 1976), this conclusion was based on the erroneous assumption that the filament linking the cell to the glass was stiff. When experiments were performed with better time-resolution (Berg, 1976; Berg *et al.*, 1982), Brownian movement of the cell body was obvious. It was implicitly assumed that this movement merely winds and unwinds the tether. What we have shown here (Figs 9 to 13) is that the cell body drifts freely: the motor does not fix the angular position of the cell, it determines torque.

When a cell is de-energized and the drive shaft is fixed by the barriers to rotation, the root-mean-square angular deviation of the cell body is of the order of $\langle\theta^2\rangle^{1/2} = 0{\cdot}06$ radians (about 3°; Berg, 1976). Were this the only mechanism contributing to fluctuations in angular position, the standard deviation in period of an energized cell would be very small. For cells spinning at the rates observed in our experiments, this standard deviation equals the time required for the cell to diffuse through 0·06 radians or, with $D_r \simeq 0{\cdot}5$ radians^2/second, about $(0{\cdot}06)^2 = 3{\cdot}6 \times 10^{-3}$ second. This is much smaller than the standard deviations that we have observed (e.g. Fig. 8). Furthermore, variations due to this mechanism would not be expected to increase with the size of the rotation interval, as they so clearly do (Figs 10, 12 and 13).

Apart from the discontinuous steps (Fig. 8) and the long-term drifts noted in the discussion of Figure 13, fluctuations attributable to torque generation were not evident. Fluctuations about the average torque, H, applied to the rotor might be caused by stochastic changes in the protonmotive force or by thermal motion in the torque-generating machinery itself. On time-scales long compared to their autocorrelation time, t_F, these fluctuations would generate a random walk in the angular position of the rotor. The standard deviation of the torque averaged over one revolution is expected to be smaller than the standard deviation of the instantaneous torque, σ_H, by a factor $(t_F/\tau)^{1/2}$, so that $\sigma_\tau/\tau = (\sigma_H/H)(t_F/\tau)^{1/2}$. Thus, contributions of processes that occur at high frequency, such as fluctuations of force-generating units about their equilibrium positions (see below), should be small. One can show, in addition, that the dependence of σ_τ on D_r and τ is not as predicted by equations (2) to (4). For example, since σ_H, H and t_F do not depend on the viscosity of the medium, σ_τ should be proportional to $\tau^{1/2}$ when cells are observed at fixed protonmotive force in media of different viscosities. This is clearly inconsistent with our results (eqn (3) and Fig. 12).

Earlier studies have shown that the motor runs at constant torque over a wide range of speeds (Manson *et al.*, 1980) and that this torque is proportional to protonmotive force over values ranging from −30 to −100 mV (Manson *et al.*, 1980; Khan & Berg, 1983). The data of Figure 6 (circles) imply that when barriers to rotation are not of concern, this proportionality holds down to nearly 0 mV. Furthermore, the torque is approximately independent of temperature and does not change when protons are replaced by deuterons (Khan & Berg, 1983). These observations argue for a mechanism in which proton flux is tightly coupled to the motion of the M ring (the rotor). They also indicate that at moderate values of Δp and viscous load, the motor operates close to thermodynamic equilibrium: the reactions that couple proton movement to movement of the M ring are so fast that they do not limit the speed of the motor.

The present study describes second-order properties of flagellar rotation and, thus, limits the class of possible mechanisms to those that allow free rotational diffusion. Our results imply that the torque generated by the motor is independent of the angular position of the M ring. In particular, this rules out certain types of stepping motors. Consider a model in which the M ring moves in discrete steps of angle ϕ separated by constant time intervals. In this case, the standard deviation of the time required for a given rotation interval will be due entirely to Brownian motion that winds and unwinds the tether. As noted above, this mechanism cannot explain the results that we have obtained.

In a more sophisticated stepping motor, the stepping times might be Poisson distributed with a mean rate v. If, in addition, the motor stepped forward or backward with a bias introduced by the protonmotive force, the cell would execute a random walk with stochastic properties similar to free Brownian movement. Fluctuations in its motion would be characterized by an effective diffusion coefficient $D_{eff} = v\phi^2/2$ (Berg, 1983). With appropriate choices of v and ϕ, D_{eff} could be comparable to the rotational diffusion coefficient of the cell body. However, if these parameters were determined solely by the internal machinery of the motor, D_{eff} would not depend on cell size or on fluidity of the medium, contrary to what we have observed (Figs 9 to 12).

In a model suggested earlier (Berg & Khan, 1983; Khan & Berg, 1983), a biased random walk is carried out by force-generating units that move rapidly from proton-binding site to proton-binding site along the periphery of the M ring, stretching and relaxing their elastic linkage to the cell wall. The motion of each unit is tightly coupled to proton translocation. At equilibrium, each unit exerts a force on the M ring proportional to Δp. This force does not suppress rotational Brownian movement: the body of a tethered cell remains free to diffuse, with a drift determined by Δp. The situation is analogous to that of a particle diffusing in a gravitational field. Thus, the predictions of this model are consistent with the results of the present study.

Appendix

The properties of the cosine transform, $C(M)$, are indicated for two different distributions of the stopping angles ϕ_j:

(1) ϕ_j distributed randomly with distribution function:

$$p(\phi) = 1/2\pi, \qquad 0 \leq \phi < 2\pi,$$

so that:

$$\langle \cos M\phi \rangle = \int_0^{2\pi} p(\phi) \cos M\phi \, d\phi = 0$$

and:

$$\langle \cos^2 M\phi \rangle = \int_0^{2\pi} p(\phi) \cos^2 M\phi \, d\phi = \frac{1}{2}.$$

Thus, from equation (1), the mean and standard deviation of the cosine transform are:

$$\langle C(M) \rangle = 0,$$

and:

$$[\langle C^2(M) \rangle - \langle C(M) \rangle^2]^{1/2} = (2n)^{-1/2}.$$

(2) ϕ_j distributed normally about the L equidistant angles $\alpha_I = (I/L)2\pi$, $I = 0, 1, \ldots, L-1$, with distribution function:

$$p(\phi) = (2\pi\sigma_\phi^2)^{-1/2} \frac{1}{L} \sum_{I=0}^{I=L-1} \times e^{-(\phi-\alpha_I)^2/2\sigma_\phi^2}, \quad -\infty < \phi < +\infty.$$

The extension of the range of ϕ to $[-\infty, +\infty]$ has a negligible effect as long as $\sigma_\phi/2\pi \ll 1$.
Then:

$$\langle \cos M\phi \rangle = \begin{cases} e^{-M^2\sigma_\phi^2/2}, & M/L \text{ integer} \\ 0, & M/L \text{ not integer} \end{cases}$$

and:

$$\langle \cos^2 M\phi \rangle = \langle (1 + \cos 2M\phi)/2 \rangle = \begin{cases} (1 + e^{-2M^2\sigma_\phi^2})/2, & 2M/L \text{ integer}, \\ 1/2, & 2M/L \text{ not integer}, \end{cases}$$

so that:

$$\langle C(M) \rangle = \begin{cases} e^{-M^2\sigma_\phi^2/2} & M/L \text{ integer}, \\ 0, & M/L \text{ not integer}, \end{cases}$$

and:

$$[\langle C^2(M) \rangle - \langle C(M) \rangle^2]^{1/2} = (2n)^{-1/2} \times \begin{cases} 1 - e^{-M^2\sigma_\phi^2}, & 2M/L \text{ even integer}, \\ (1 + e^{-2M^2\sigma_\phi^2})^{1/2}, & 2M/L \text{ odd integer}, \\ 1, & 2M/L \text{ not integer}. \end{cases}$$

Note that for $M\sigma_\phi \gg 1$ (large M), the spectrum approaches that of a random distribution with vanishing mean and root-mean-square noise $(2n)^{-1/2}$. Also, one can find σ_ϕ from the primary and secondary maxima:

$$\sigma_\phi = \frac{1}{L} \left\{ \frac{2}{3} \ln [\langle C(L) \rangle / \langle C(2L) \rangle] \right\}^{1/2}.$$

We thank John Hopfield for discussions, David Trentham for supplying the photolytic compound, Henry Lester for use of flash equipment, Jeff Segall for help with iontophoresis, and Steve Block for help with calibration of the video system. This work was supported by grant PCM-8215126 from the U.S. National Science Foundation.

References

Armitage, J. P. & Evans, M. C. W. (1982). *Biochem. Soc. Trans.* **10**, 418.

Belyakova, T. N., Glagolev, A. N. & Skulachev, V. P. (1976). *Biochemistry*, **41**, 1206–1210 (1976). Translated from: *Biokhimiya*, **41**, 1478–1483.

Berg, H. C. (1974). *Nature (London)*, **249**, 77–79.

Berg, H. C. (1975). *Nature (London)*, **254**, 389–392.

Berg, H. C. (1976). In *Cell Motility* (Goldman, R., Pollard, T. & Rosenbaum, J., eds), vol. 3, pp. 47–56, Cold Spring Harbor Laboratory Press, Cold Spring Harbor.

Berg, H. C. (1983). *Random Walks in Biology*, pp. 81–85, Princeton University Press, Princeton, New Jersey.

Berg, H. C. & Anderson, R. A. (1973). *Nature (London)*, **245**, 380–382.

Berg, H. C. & Block, S. M. (1984). *J. Gen. Microbiol.* **130**, 2915–2920.

Berg, H. C. & Khan, S. (1983). In *Motility and Recognition in Cell Biology* (Sund, H. & Veeger, C., eds), pp. 486–497, Walter de Gruyter, Berlin.

Berg, H. C. & Turner, L. (1979). *Nature (London)*, **278**, 349–351.

Berg, H. C., Manson, M. D. & Conley, M. P. (1982). *Proc. Symp. Soc. Exp. Biol.* **35**, 1–31.

Block, S. M. & Berg, H. C. (1984). *Nature (London)*, **309**, 470–472.

Block, S. M., Segall, J. E. & Berg, H. C. (1982). *Cell*, **31**, 215–226.

Block, S. M., Segall, J. E. & Berg, H. C. (1983). *J. Bacteriol.* **154**, 312–323.

DePamphilis, M. L. & Adler, J. (1971). *J. Bacteriol.* **105**, 384–395.

Dimmitt, K. & Simon, M. (1971). *J. Bacteriol.* **105**, 369–375.

Glagolev, A. N. & Skulachev, V. P. (1978). *Nature (London)*, **272**, 280–282.

Khan, S. & Berg, H. C. (1983). *Cell*, **32**, 913–919.

Kihara, M. & Macnab, R. M. (1981). *J. Bacteriol.* **145**, 1209–1221.

Larsen, S. H., Adler, J., Gargus, J. J. & Hogg, R. W. (1974). *Proc. Nat. Acad. Sci., U.S.A.* **71**, 1239–1243.

Manson, M. D., Tedesco, P., Berg, H. C., Harold, F. M. & van der Drift, C. (1977). *Proc. Nat. Acad. Sci., U.S.A.* **74**, 3060–3064.

Manson, M. D., Tedesco, P. M. & Berg, H. C. (1980). *J. Mol. Biol.* **138**, 541–561.

Matsuura, S., Shioi, J.-I. & Imae, Y. (1977). *FEBS Letters*, **82**, 187–190.

McCray, J. A. & Trentham, D. R. (1985). *Biophys. J.* **47**. 406a.

Repaske, D. R. & Adler, J. (1981). *J. Bacteriol.* **145**, 1196–1208.

Segall, J. E., Manson, M. D. & Berg, H. C. (1982). *Nature (London)*, **296**, 855–857.

Silverman, M. & Simon, M. (1974). *Nature (London)*, **249**, 73–74.

Skulachev, V. P. (1975). In *Enzymes, Electron Transport Systems. Proc. Tenth FEBS Meet.* (Desnuelle, P. & Michelson, A. M., eds), vol. 40, pp. 225–238, North-Holland, Amsterdam.

van der Drift, C., Duiverman, J., Bexkens, H. & Krijnen, A. (1975). *J. Bacteriol.* **124**, 1142–1147.

Wagenknecht, T., DeRosier, D. J., Aizawa, S.-I. & Macnab, R. M. (1981). *J. Mol. Biol.* **162**, 69–87.

Edited by H. E. Huxley